

# Study of Multiparticle Azimuthal Correlations in Central CNe, MgMg, CCu and OPb Interactions at Energy of 3.7 GeV per Nucleon

L.Chkhaidze, T.Djobava, L.Kharkhelaury

*High Energy Physics Institute of Tbilisi State University, Georgia*

*Corresponding author's E-mail: ida@sun20.hepi.edu.ge or*

*lali@sun20.hepi.edu.ge*

## ABSTRACT

Azimuthal correlations between protons and between pions have been investigated in central CNe, MgMg, CCu and OPb collisions at energy of 3.7 GeV/nucleon. "Back-to-back" (negative) correlations have been observed for protons in CNe, CCu and for  $\pi^-$ -mesons in CNe and MgMg collisions. For  $\pi^-$ -mesons "side-by-side" (positive) azimuthal correlations have been observed for heavy systems of CCu and OPb. The Quark Gluon String Model satisfactorily describes the experimental results both for protons and  $\pi^-$ -mesons.

PACS numbers: 25.70.-z; 25.75.Ld

## 1. INTRODUCTION

Relativistic nucleus–nucleus collisions are very well suited for investigation of excited nuclear matter properties which are the subject of intense studies both experimentally and theoretically. Theoretical models predict formation of exotic states of nuclear matter, for example the phase transition to a quark-gluon plasma [1,2]. One of the main goals of relativistic heavy-ion collision experiments is to study nuclear matter under extreme conditions of high densities and temperatures. The most impressive results of high energy heavy ion research so far are new collective phenomena discovered in these reactions. Study of multiparticle correlations offers unique information about space-time evolution of the collective system. During last years an intensive analysis of experimental data have been carried out using the collective variables, which depend on the momentum of all secondary particles, to reveal a nontrivial effects in nucleus–nucleus collisions.

Experimental discovery of such transitions is impossible without understanding of the mechanism of collisions and studying the characteristics of multiparticle production in nucleus–nucleus interactions. Multiparticle correlations had been investigated at the first time at the BEVALAC more than 10 years ago [3].

In this article we present results of the analysis of multiparticle correlations in central CNe, MgMg, CCu and OPb collisions at energy of 3.7 GeV/nucleon. Azimuthal correlations between protons and between pions and dependence of these correlations on the projectile ( $A_P$ ) and target ( $A_T$ ) nucleus have been investigated.

## 2. EXPERIMENT

Data were obtained using the  $4\pi$  spectrometer SKM-200 – GIBS of the Dubna JINR [4,5]. The SKM-200 – GIBS set-up consists of a 2 m streamer chamber with fiducial volume of a  $2\times 1\times 0.6$  m<sup>3</sup>, placed in a magnetic field of  $\sim 0.8$  T ( $\sim 0.9$  T for MgMg) and a triggering

system. The streamer chamber was exposed to beams of C, O and Mg nuclei accelerated in the synchrotron up to energy of 3.7 GeV per incident nucleon. Solid targets in the form of thin discs with thickness  $(0.2\div 0.5)$  g/cm<sup>2</sup> (the thickness of Mg was 1.5 g/cm<sup>2</sup>; neon-gas filling of the chamber also served as a nuclear target) were mounted inside the chamber at a distance of 70 cm from the entrance window and at a height of 8 cm above the middle electrode. Photographs of the events were taken using an optical system with 3 objectives. Experimental set-up and the logic of the triggering system are presented in Fig. 1. Triggering system allowed the selection of "inelastic" and "central" collisions.

The "inelastic" trigger, consisting of two sets of scintillation counters mounted upstream ( $S_1 - S_4$ ) and downstream ( $S_5, S_6$ ) the chamber, has been selected all inelastic interactions of incident nuclei on a target.

The "central" triggering system was consisting of the same upstream part as in the "inelastic" system and of scintillation veto counters ( $S_{ch}, S_n$ ), to reject a projectile and its charged and neutral spectator fragments, in the downstream part. All counters were made from plastic scintillators and worked with photomultipliers PM-30. The  $S_1$  counter with the scintillator of  $20\times 20\times 0.5$  cm<sup>3</sup> size, worked in the amplitude regime and identified the beam nuclei by its charge. The nuclei from the beam, going to the target, have been selected using the profile counters  $S_2, S_3$  with the plastic of 0.15 mm diameter and 3 mm thickness and "thin" counter  $S_4$  (15 mm and 0.1 mm correspondingly). The  $S_{ch}$  counters (two counters with plastic of  $40\times 40\times 0.5$  cm<sup>3</sup> size) were placed at a distance of 4 m downstream from the target and registered secondary charged particles, emitted from the target within a cone of half angle  $\theta_{ch} = 2.4$  grad or 2.9 grad. The  $S_n$  counters were registering the neutrons, emitted from the target in the same solid angle  $\theta_n = 2.4$  grad or 2.9 grad.. The  $S_n$  telescope consisted of the five counters of  $40\times 40\times 2$  cm<sup>3</sup> size, layered by 10 cm thick iron blocks. The central trigger was selecting events defined as those with no charged projectile spectator fragments and spectator neutrons ( $p/Z > 3$  GeV/c) emitted at angles  $\theta_{ch} = \theta_n = 2.4$  grad or 2.9 grad. ( $\sim 4$ msr). The trigger efficiency was 99 % and 80 % for charged and neutral projectile fragments, respectively. The trigger mode for each exposure is defined as  $Tr(\theta_{ch}, \theta_n)$  ( $\theta_{ch}$  and  $\theta_n$  expressed in degrees and rounded to the closest integer value). Thus nucleus-nucleus interactions obtained with this set-up correspond to the following  $Tr(\theta_{ch}, \theta_n)$  triggers: CNe

– Tr(2, 0), MgMg – Tr(2, 2), CCu – Tr(2, 0) and Tr(3, 3), OPb – Tr(2, 0).

Biases and correction procedures were discussed in detail in [4,5]. The ratio  $\sigma_{\text{cent}}/\sigma_{\text{inel}}$  (that characterizes the centrality of selected events) is  $(9\pm 1)\%$  for CNe and  $(21\pm 3)\%$  for CCu and the fraction of central MgMg events is  $\approx 4\times 10^{-4}$  among all inelastic interactions. Average momenta measurement errors  $\langle \Delta p/p \rangle = (8\div 10)\%$  for protons and  $5\%$  for pions, corresponding errors of the production angles are  $\Delta\theta = (1\div 2)$  grad. and  $0.5$  grad. ( for  $\pi^-$ -mesons in MgMg interactions we had  $\langle \Delta p/p \rangle = 1.5\%$ ,  $\Delta\theta = 0.3$  grad.)

### 3. QUARK GLUON STRING MODEL

Several theoretical models of nucleus–nucleus collisions at high energy have been proposed in Refs. [6-8]. These models allow one to test various assumptions concerning the mechanism of particle production at extreme conditions achieved only in nucleus–nucleus collisions. The Quark Gluon String Model (QGSM) has been used for the comparison with our experimental results. QGSM is presented in detail in papers [9,10]. The QGSM is based on the Regge and string phenomenology of particle production in inelastic binary hadron collisions. For description the evolution of the hadron and quark-gluon phases, uses a coupled system of Boltzmann-like kinetic equations. Nuclear collisions are treated as a mixture of independent interactions of the projectile and target nucleons, stable hadrons and short lived resonances. The QGSM includes low mass vector mesons and baryons with spin  $3/2$ , mostly  $\Delta(3/2, 3/2)$  via resonant reactions. Pion absorption by  $NN$  quasideuteron pairs is also taken into account. The coordinates of nucleons are generated according to a realistic nuclear density. The sphere of the nucleus is filled with the nucleons at a condition that the distance between them is greater than  $0.8$  fm. The nucleon momenta are distributed in the range of  $0 \leq p \leq p_F$ . The maximum nucleon Fermi momentum is

$$p_F = (3\pi^2)^{1/3} h \rho^{1/3}(r) \quad (1)$$

where  $h=0.197$  fm·GeV/ $c$ ,  $\rho(r)$  is nuclear density.

The procedure of event generation consists of three steps: the definition of configurations of colliding nucleons, production of quark-gluon strings and fragmentation of strings (breakup) into observed hadrons. The model includes also the formation time of hadrons. The QGSM has been extrapolated to the range of intermediate energy ( $\sqrt{s} \leq 4$  GeV) to use it as a basic process during the generation of hadron-hadron collisions. Masses of "strings" produced at  $\sqrt{s} = 3.6$  GeV were small (usually not greater than 2 GeV), and they were fragmenting mainly ( $\approx 90$  %) through two-particle decays. For main  $NN$  and  $\pi N$  interactions the following topological quark diagrams [7] were used: binary, "undeveloped" cylindrical, diffractive and planar. The binary process makes a main contribution which is proportional to  $1/p_{\text{lab}}$ . It corresponds to quark rearrangement without direct particle emission in the string decay. This reaction predominantly results in the production of resonances (for instance,  $p + p \rightarrow N + \Delta^{++}$ ), which are main source of pions. The comparable contributions to the inelastic cross section, which however decreases with decreasing  $p_{\text{lab}}$ , come from the diagrams corresponding to the "undeveloped" cylindrical diagrams and from the diffractive processes. Transverse momenta of pions produced in quark-gluon string fragmentation processes are the product of two factors: string motion on the whole as a result of transverse motion of constituent quarks and  $q\bar{q}$  production in string breakup. The transverse motion of quarks inside hadrons was described by the Gaussian distribution with variance  $\sigma^2 \approx 0.3$  (GeV/c)<sup>2</sup>. Transverse momenta  $k_T$  of produced  $q\bar{q}$  in the c.m.s. of the string follow the dependence:

$$W(k_T) = 3B/\pi(1 + Bk_T^2)^4 \quad (2)$$

where  $B = 0.34$  (GeV/c)<sup>-2</sup>.

The cross section of hadron interactions were taken from experiments. Isotopic invariance and predictions of the additive quark model [11] (for meson-meson cross sections, etc.) were used to avoid data deficiency. The resonance cross sections were assumed to be identical to the stable particle cross sections with the same quark content. For the resonances the tabulated widths were used.

The QGSM simplifies the nuclear effects. In particular, coupling of nucleons inside the nucleus is neglected, and the decay of excited recoil nuclear fragments and coalescence of nucleons is not included.

We have generated CNe, CCu, OPb and MgMg interactions using the Monte Carlo generator COLLI, which is based on the QGSM and then traced through the detector and trigger filter. In the generator COLLI there are two possibilities to generate events: 1) at not fixed impact parameter  $\tilde{b}$  and 2) at fixed  $b$ . From the impact parameter distributions we obtained the mean value of  $\langle b \rangle = 2.2$  fm, 1.3 fm, 2.7 fm and 3.7 fm for CNe, MgMg, CCu and OPb collisions. For the obtained values of  $\langle b \rangle$  we have generated a total sample of events 6270, 9320, 2430 and 6200, respectively.

The QGSM overestimate the production of low momentum protons with  $p < 0.2$  GeV/c, which are mainly the target fragments and were excluded from the analysis. From the analysis of generated events protons with deep angles greater than 60 grad. had been excluded, because in the experiment the registration efficiency of such vertical tracks is low.

#### 4. AZIMUTHAL CORRELATIONS BETWEEN PROTONS AND BETWEEN PIONS

In Refs. [12,13] the procedure to study of the correlation between groups of particles has been developed. The azimuthal correlation function was defined by the relative opening angle between the transverse momentum vector sums of particles emitted forward and backward with respect to the rest frame of the target nucleus ( $y_t = 0.2$ ).

We have applied this method for our data, but the analysis have been carried out in the central rapidity region instead of the target rapidity range of Refs. [12,13]. The analysis have been performed event by event, in each event we denote the vectors:

$$\mathbf{Q}_B = \sum_{y_i < \langle y \rangle} \mathbf{P}_{\perp i} \quad (3)$$

and

$$\mathbf{Q}_F = \sum_{y_i \geq \langle y \rangle} \mathbf{P}_{\perp i} \quad (4)$$

where  $\langle y \rangle$  is the average rapidity in each event.

Then the correlation function  $C(\Delta\varphi)$  is constructed as follows:

$$C(\Delta\varphi) = dN/d\Delta\varphi \quad (5)$$

where  $\Delta\varphi$  is the angle between the vectors  $\mathbf{Q}_B$  and  $\mathbf{Q}_F$ :

$$\Delta\varphi = \arccos(\mathbf{Q}_B \cdot \mathbf{Q}_F) / (|\mathbf{Q}_B| \cdot |\mathbf{Q}_F|). \quad (6)$$

Essentially,  $C(\Delta\varphi)$  measures whether the particles in the backward and forward hemispheres are preferentially emitted "back-to back" ( $\Delta\varphi = 180$  grad.) or "side-by-side" ( $\Delta\varphi = 0$  grad.) [12]. The protons from CNe and CCu collisions have been analysed with use of this method.

For the analysis it is necessary to perform an identification of  $\pi^+$  mesons, the admixture of which amongst the charged positive particles is about (25÷27)% . The statistical method have been used for identification of  $\pi^+$  mesons. The main assumption is based on the similarity of spectra of  $\pi^-$  and  $\pi^+$  mesons ( $n_\pi, p_T, p_L$ ). The two-dimensional distribution of ( $p_T, p_L$ ) variables have been used for identification of  $\pi^+$  mesons. The whole plane is divided into 7 zones. For example, for CNe collisions:

- 1)  $p_L > 2.5$  GeV/ $c$  or  $p_T > 0.9$  GeV/ $c$ ;
- 2)  $0 \leq p_L \leq 1.4$  GeV/ $c$  and  $p_T \leq 0.7$  GeV/ $c$  – PMAX;
- 3)  $0 \leq p_L \leq 1.4$  GeV/ $c$  and  $p_T > 0.7$  GeV/ $c$ ;
- 4)  $1.4$  GeV/ $c < p_L < 2.5$  GeV/ $c$ ;
- 5)  $-0.2 \leq p_L \leq 0$  GeV/ $c$  and  $p_T \leq 0.3$  GeV/ $c$ ;
- 6)  $-0.2 \leq p_L \leq 0$  GeV/ $c$  and  $p_T > 0.3$  GeV/ $c$ ;
- 7)  $p_L < -0.2$  GeV/ $c$ .

The zone 2 of maximal overlap – PMAX, in its turn, is divided into  $7 \times 7 = 49$  cells. The probability of hitting each zone and respectively the cell by  $\pi^-$  mesons and charged positive particles is defined and the relative probability of hitting of  $\pi^-$  mesons is calculated as a result. The admixture of  $\pi^+$  mesons in the zone 1 is negligible. The procedure of dividing the ( $p_T, p_L$ ) plane into the cells allows to simplify the mathematical algorithm and improves the accuracy of the identification. In Fig. 2 the division of the ( $p_T, p_L$ ) plane is presented for CNe collisions. It was assumed, that  $\pi^+$  and  $\pi^-$  mesons hit given cell with equal probability ( the equal probability densities for  $\pi^+$  and  $\pi^-$  were assumed).



The identification in fact is equal to summing of hitting probabilities into each cell and when the sum reaches the critical value, the particle is considered as  $\pi^+$  meson. The rest of particles are assumed to be protons. For each proton and  $\pi^+$  meson the sign is recorded on DST (Data Summar Tape), which indicates to which zone of  $(p_T, p_L)$  plane belongs the given particle and what is the probability. Particles with  $p_T > 0.9$  GeV/c or  $p_L > 2.5$  GeV/c are unambiguous protons with probability equal to 1.

After identification of  $\pi^+$  mesons in the event, the difference of  $\pi^+$  and  $\pi^-$  mesons  $\Delta n$  is determined. If  $|\Delta n| > 2$ , in the region PMAX the identification  $\pi^+ \leftrightarrow$  proton is interchanged and for that reason particles with smaller probability are chosen. If the condition of approachment of multiplicities is not fulfilled, then in this case into the "head" information of the event such a sign is recorded, which allows to exclude the given event from the further analysis.

After performed identification the admixture of  $\pi^+$  mesons amongst the protons is not exceeding  $(5 \div 7)\%$ . The mean values of multiplicity, momentum and transverse momentum for  $\pi^+$  and  $\pi^-$  mesons are presented in Tabl. 1. One can see, that the average kinematical characteristics of  $\pi^+$  and  $\pi^-$  mesons coincide within the errors satisfactorily.

The numbers of events for CNe and CCu collisions and the mean rapidities of analysed protons  $\langle y \rangle$  are listed in Tabl. 2. Fig. 3 shows the experimental correlation function  $C(\Delta\varphi)$  for protons from central CNe and CCu collisions. One can observe from Fig. 3 a clear correlation for protons (correlation increases with  $\Delta\varphi$ , reaches maximum at  $\Delta\varphi = 180$  grad.). To quantify these experimental results, the data were fitted by:

$$C(\Delta\varphi) = 1 + \xi \cos(\Delta\varphi). \quad (7)$$

Results of the fitting are listed in Tabl. 2. The strength of the correlation is defined as

$$\zeta = C(0 \text{ grad.})/C(180 \text{ grad.}) = (1 + \xi)/(1 - \xi). \quad (8)$$

As it can be seen from the Tabl. 2, the asymmetry coefficient  $\xi < 0$  and thus the strength of correlation  $\zeta < 1$  for protons in both CNe and CCu interactions, meaning the negative correlations and that protons are preferentially emitted back-to-back. Absolute values of  $\xi$  increase and  $\zeta$  decrease with target mass increases.

A similar negative (back-to-back) correlation have been observed by Plastic Ball collaboration at Bevalac between the "slow" ( $40 < E < 240$  MeV) and the "fast" ( $E > 240$  MeV) fragments for symmetric ( $^{40}\text{Ca} + ^{40}\text{Ca}$ ,  $^{93}\text{Nb} + ^{93}\text{Nb}$ ) and asymmetric ( $^{20}\text{Ne} + ^{93}\text{Pb}$ ) pairs of nuclei in the energy interval of 0.4 to 1 GeV/nucleon [14,15] and also between protons in  $p + \text{Au}$  collisions at energy of 4.9 GeV/nucleon [12,13]. The investigation of large angle two-particle correlations [16], have been carried out at Dubna for collisions of  $^4\text{He}$  and  $^{12}\text{C}$  with different nuclear targets ( $^{27}\text{Al}$ ,  $^{64}\text{Cu}$  and  $^{93}\text{Pb}$ ) at energy of 3.6 GeV/nucleon. For protons and deuterons, negative (back-to-back) correlation was observed for all targets. In CC inelastic interactions at a momentum of 4.2 GeV/c/nucleon in the 2-meter Propan Bubble Chamber of JINR [17] the back-to-back azimuthal correlations between the groups of the particles (protons) emitted in the forward and backward hemispheres in the c.m.s. of the collisions (see Fig. 5a [17]) have been obtained. Protons showed a typical back-to-back (negative) correlation in the  $p$  -,  $\text{O}$  -, and  $\text{S}$  - induced reactions on different nuclei ( $\text{Au}$ ,  $\text{Ag}$ ,  $\text{Al}$ ,  $\text{C}$ ) at the CERN-SPS (WA80 collaboration) at energy of 60 and 200 GeV/nucleon [12,13]. Azimuthal correlations in the target rapidity range of  $0.1 \leq y_0 \leq 0.3$  have been obtained and within these limits no significant change of the correlation functions has been observed. We have studied the strength of the correlation functions in central CNe and CCu collisions for different rapidities ( $y_0$ ) and emission angle ( $\theta$ ) intervals in the l. s. (see Tabl. 3). One can see from the Tabl. 3 that absolute values of asymmetry coefficient decrease from central rapidity region to the target fragmentation range.

The back-to back (negative) emission of protons can be understood as resulting from (local) total momentum conservation [13]. This behaviour is in a good agreement with collective nuclear matter flow concept [16].

In view of the strong coupling between the nucleons and pions, it is interesting to know the origin of correlations between pions. The  $\pi^-$ -mesons in our experiment have been identified practically unambiguously, the admixture of  $e^-$ ,  $\bar{p}$  and  $K^-$ -mesons is almost negligible [4]. We have studied also correlations between  $\pi^-$ -mesons. For CNe interactions into the analysis  $\pi^+$  mesons have been included also in order to increase the multiplicity in each event. Correlation functions for  $\pi^-$ -mesons in CNe, MgMg, CCu and OPb interactions are presented in Fig. 4. One can observe from Fig. 4a a clear back-to-back ( $\xi < 0$ ,  $\zeta < 1$ , i.e. negative) correlations

for pions for light system of CNe (analogy as for the protons in CNe collisions). Study of interactions of the symmetric pair of nuclei MgMg (6239 collisions, 50775  $\pi^-$ -mesons) gives the possibility of a better manifestation of nuclear effects then for the asymmetric pairs of nuclei. For MgMg collisions a back-to-back pion correlations had been obtained only for the events with multiplicity  $n_- > 7$  and no correlations for  $n_- \leq 7$  (Fig. 4a).

For heavy, asymmetric pairs of nuclei CCu and OPb the side-by-side ( $\xi > 0$  and  $\zeta > 1$ , i.e. positive) correlations of pions can be seen from Fig. 4b. Similar, side-by-side correlations of pions have been observed in  $p + Au$  collisions at Bevalac (4.9 GeV/nucleon) and CERN-SPS (60 and 200 GeV/nucleon) energies [12, 13]. These results agree with that of Refs. [18, 19]. Large angle two-particle correlations carried out at energy of 3.6 GeV/nucleon at JINR [18] for  $^4\text{He}$ - and  $^{12}\text{C}$ -beams, showed the negative (back-to-back) pion correlations for light (Al) and the positive (side-by-side) correlations for the heavy target (Pb) (no correlation for a medium target Cu).

One can see from Tables 2 and 4 the absolute values of the asymmetry coefficient ( $|\xi|$ ) increase and the strength of correlations ( $\zeta$ ) decrease while target mass increases for both protons and pions back-to-back (negative) correlations in contrast to the results of Ref. [13], where back-to-back asymmetry of protons tends to vanish with increase of target mass in proton induced reactions at 200 GeV/c (see Fig. 4 [13]). For side-by-side (positive) correlations of pions in CCu and OPb collisions  $\xi$  and  $\zeta$  increase with the target mass due to the increasing amount of matter in their path.

The reason for the observed difference behaviour between protons and pions comes from the pion absorption in the excited target matter ( $\pi + N \rightarrow \Delta$  and  $\Delta + N \rightarrow N + N$ ) [12, 13]. While the back-to-back emission of protons can be understood as resulting from transverse momentum conservation, the pion correlations show, in the data, an opposite behaviour. The side-by-side correlation of pions can naturally be explained based on the picture that pions, which are created in collision at a  $b \neq 0$  fm ( $b$  is the impact parameter) either suffer rescattering or even complete absorption in the target spectator matter. Both processes will result in a relative depletion of pions in the geometrical direction of the target spectator matter and hence will cause an azimuthal side-by-side (positive) correlation as observed in the experimental data. This picture is further supported by calculations within

the framework of the RQMD model [20] , which includes pion absorption by excited nuclear matter based on experimentally measured cross sections.

The QGSM yields a significant azimuthal correlations, which follow trends similar to the experimental data (Figs. 3, 4).

To be convinced, that the azimuthal correlations in Figs. 3, 4 (for both experimental and QGSM data) between protons and between pions are due to correlations between these particles and can not be the result of detector biases or finite-multiplicity effects, we obtained data for dependence of  $C(\Delta\psi)$  on  $\psi$  for secondaries, where  $\psi$  is the angle between the transverse momentum of each particle emitted in the backward (forward) hemisphere and  $\mathbf{Q}_B$  ( $\mathbf{Q}_F$ ) vector, respectively. One can see from Fig. 5, that there is no correlation for CCu interactions both for protons (Fig. 5a) and for pions (Fig. 5b). Similar results have been obtained for CNe collisions too.

As obtained in our previous articles [21–23], the dependence of the mean transverse momentum in the reaction plane  $\langle P_X \rangle$  on the normalized rapidity  $y/y_p$  in the l. s. showed the typical *S*-shape behaviour in CNe and CCu collisions for protons and pions. For CNe collisions  $\langle P_X \rangle$  for pions is directed in the same direction as for protons, i.e. flows of protons and pions are correlated, while for CCu interactions the  $\langle P_X \rangle$  of  $\pi^-$ -mesons is directed oppositely to that of the protons (antiflow) (see Fig. 1 [22]). In MgMg central collisions [24], for  $\pi^-$ -mesons with multiplicity  $n_- > 7$  the dependence of  $\langle P_X(Y) \rangle$  on  $Y$  exhibits *S*-shape behaviour similar to the form of the  $\langle P_X \rangle$  spectra for protons and pions in central CNe collisions.

In order to extend these investigations, we have obtained the relation between  $\langle P_X \rangle^2$  and the angle  $\varphi$ , where  $\varphi$  is the opening angle between  $\mathbf{Q}_B$  and  $\mathbf{Q}_F$  vectors. One can see from Fig. 6, that for protons in CNe and CCu collisions, the distributions show *S*-shape behaviour and slopes of distributions increase with target mass. One can see from Fig. 6 that at  $\varphi = 90$  grad. the values of  $\langle P_X \rangle$  not depend on  $A_T$ .

#### 4. CONCLUSION

The study of azimuthal correlations between protons and between pions in central CNe, MgMg, CCu and OPb collisions have been carried out.

1. For protons a "back-to back" (negative) correlations were observed in CNe and CCu interactions. The asymmetry coefficient  $\xi$  ( $\xi < 0$ ) increases and the strength of correlation  $\zeta$  ( $\zeta < 1$ ) decreases with increase of the target mass.

2. A "back-to-back" pion correlations had been obtained for a light, symmetric pairs of nuclei (CNe and MgMg), where  $\xi$  and  $\zeta$  parameters have the same behaviour as for protons.

3. For heavy pairs of nuclei (CCu and OPb) "side-by-side" (positive) pion correlation were observed. The asymmetry coefficient ( $\xi > 0$ ) and the strength of correlations ( $\zeta > 1$ ) increase with increase of projectile ( $A_P$ ) and target ( $A_T$ ) mass.

4. The dependence of the square of the mean transverse momentum in the reaction plane  $\langle P_X \rangle^2$  on  $\varphi$  (the angle between the vector sums of the forward and backward emitted particles) shows S-shaped behaviour. Slopes of distributions increase with target mass.

5. The QGSM satisfactorily describes azimuthal correlations of protons and  $\pi^-$ -mesons for all pairs of nuclei.

**ACKNOWLEDGEMENTS** We would like to thank M.Anikina, A.Golokhvastov, S.Khorozov and J.Lukstins for fruitful collaboration during the obtaining of the data. We are very grateful to Z. Menteshashvili for reading the manuscript.

## References

- [1] M. Jacob and Van Than Tran, Phys. Rev. C **88**, 725 (1980).
- [2] H. Stöcker, *et al.*, Phys. Lett. B **81**, 303 (1979).
- [3] H. A. Gustafsson, *et al.*, Phys.Lett. B **142**, 141 (1984).
- [4] M. Anikina, *et al.*, Preprint No. E1-84-785, JINR (Dubna, (1984).
- [5] M. Anikina, *et al.*, Phys.Rev. C **33**, 895 (1986).
- [6] S. Nagamiya and M. Gyalassy., Adv. in Nucl. Phys. **13**, 201 (1984).
- [7] B. A. Li, W. Bauer, and G. Bertsch, Phys.Rev. C **44**, 450 (1991).
- [8] M. D. Zubkov., Yad. Fiz. **55**, 455 (1989).
- [9] N. Amelin, *et al.*, Yad. Fiz. **52**, 272 (1990).
- [10] N. Amelin, *et al.*,Phys. Rev. C **44**, 1541 (1991).
- [11] V. V. Anisovich, *et al.*, Nucl. Phys. B **133**, 477 (1978).
- [12] H. R. Schmidt, *et al.*, Nucl. Phys. A **544**, 449 (1992).
- [13] T. C. Awes, *et al.*, Phys. Lett. B **381**, 29 (1996).
- [14] H. A. Gustafsson, *et al.*, Z. Phys. A **321**, 389 (1985).
- [15] P. Beckmann, *et al.*, Modern Phys. Lett. A **2**, 169 (1987).
- [16] B. P. Aduasevich, *et al.*, Nucl. Phys. B **316**, 419 (1990);  
B. P. Aduasevich, *et al.*, Yad. Fiz. **57** 268 (1994).
- [17] A. Kh. Vinitzky, *et al.*, Yad. Fiz. **54**, 12 (1991).
- [18] B. P. Aduasevich, *et al.*, Yad. Fiz. **57**, 2057 (1994).

- [19] H. Sorge, *et al.*, Z. Phys. **644**, 609 (1990).
- [20] Th. Lister, *et al.*, Preprint No. 94-1, GSI (University of Munster, 1994).
- [21] L. Chkhaidze, *et al.*, Phys.Lett. B **411**, 26 (1997).
- [22] L. Chkhaidze, *et al.*, Phys.Lett. B **479**, 21 (2000).
- [23] L. Chkhaidze, *et al.*, nucl-ex/0008001, 2000; submitted to Eur. Phys. J.
- [24] L. Chkhaidze, *et al.*, Eur. Phys. J. A **1**, 2996 (1998).

## FIGURE CAPTIONS

**Fig.1.** Experimental set-up. The trigger and trigger distances are not to scale.

**Fig.2** Two dimensional  $(p_T, p_L)$  ( $p_T$  and  $p_L$  denote the transverse and longitudinal momenta, correspondently) plot for the identificaton of protons and  $\pi^+$  mesons in CNe collisions.

**Fig.3.** The dependence of the correlation function  $C(\Delta\varphi)$  on the  $\varphi$  for protons from: (o) – CNe and ( $\Delta$ ) – CCu collisions. ( $\times$ ) – the QGSM data. Dashed curves are the results of the approximation of the data (see text).

**Fig.4.** The dependence of the correlation function  $C(\Delta\varphi)$  on the  $\varphi$  for  $\pi^-$ -mesons from: (a) (o) – CNe, ( $\bullet$ ) – MgMg ( $n_- > 7$ ), ( $\diamond$ ) – MgMg ( $n_- \leq 7$ ) and (b) ( $\Delta$ ) – C-Cu, ( $\oplus$ ) – OPb collisions. ( $\times$ ,  $\star$ ) – the QGSM data, correspondently. Solid and dashed curves are the results of the approximation of the data (see text).

**Fig.5.** The dependence of the correlation function  $C(\Delta\psi)$  on the  $\psi$  in CCu collisions for protons (a) and for  $\pi^-$ -mesons (b). (o) – for particles emitted in the backward hemisphere, ( $\Delta$ ) – for particles emitted in the forward hemisphere. ( $\times$ ) – the QGSM data. Curves are the results of the approximation of the data by the first order polynoms.

**Fig.6.** The dependence of  $\langle P_x \rangle^2$  on  $\varphi$  (as described in the text) for protons in: (o) – CNe and ( $\Delta$ ) – CCu collisions. ( $\times$ ,  $\star$ ) – the QGSM data, correspondently. Solid curves are the results of the approximation of the data by 4th order polynoms.



Table 1. The number  $\pi^+$  and  $\pi^-$  mesons and their average kinamatical characteristics in CNe and CCu collisions after the identification of protons and  $\pi^+$  mesons.

$A_P - A_T$	Particle Type	$N_\pi$	$\langle n_\pi \rangle$	$\langle p_T \rangle$ GeV/c	$\langle p \rangle$ GeV/c
CNe	$\pi^+$	3089	$4.26 \pm 0.06$	$0.234 \pm 0.003$	$0.600 \pm 0.009$
	$\pi^-$	3120	$4.31 \pm 0.07$	$0.226 \pm 0.005$	$0.612 \pm 0.009$
CCu	$\pi^+$	3713	$5.74 \pm 0.09$	$0.222 \pm 0.003$	$0.522 \pm 0.008$
	$\pi^-$	3635	$5.68 \pm 0.10$	$0.213 \pm 0.005$	$0.508 \pm 0.009$

Table 2. The number of experimental events ( $N_{\text{event}}$ ) and participant protons ( $N_{\text{prot.}}$ ), the asymmetry coefficient ( $\xi$ ), the strength of the correlation ( $\zeta$ ) and the mean rapidity ( $\langle y \rangle$ ) of protons.

$A_P - A_T$	$N_{\text{event}}$	$N_{\text{prot.}}$	$\xi$	$\zeta$	$\langle y \rangle$
CNe	723	9201	$-0.23 \pm 0.05$	$0.63 \pm 0.09$	$1.07 \pm 0.07$
CCu	663	12715	$-0.35 \pm 0.05$	$0.48 \pm 0.06$	$0.73 \pm 0.05$

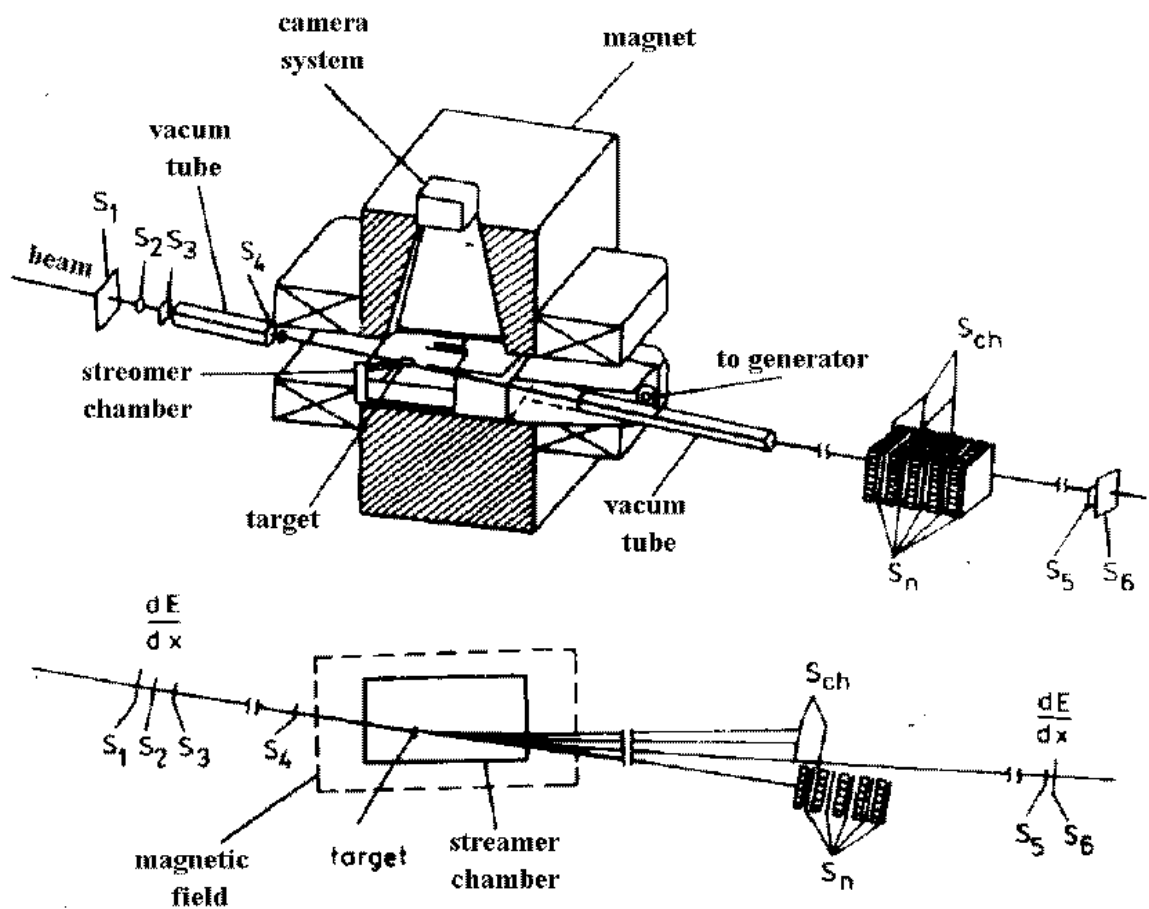
Table 3. Values of the coefficient of asymmetry ( $\xi$ ) for protons in CNe and CCu collisions for different intervals of emission angle ( $\theta$ ) and rapidity ( $y_0$ ).

coeff. of asymm.	range		CNe	CCu
$\xi$	in central region $0.5 \leq y_0 \leq 2.5$		$-0.23 \pm 0.05$	$-0.35 \pm 0.05$
	$10 \text{ grad} \leq \theta \leq 180 \text{ grad.}$	$y_0=0.2$	–	$-0.22 \pm 0.05$
		$y_0=0.3$	$-0.11 \pm 0.03$	$-0.27 \pm 0.05$
	$20 \text{ grad} \leq \theta \leq 180 \text{ grad.}$	$y_0=0.2$	–	$-0.13 \pm 0.05$
		$y_0=0.3$	–	$-0.19 \pm 0.05$
	$30 \text{ grad} \leq \theta \leq 180 \text{ grad.}$	$y_0=0.2$	–	$-0.07 \pm 0.01$
		$y_0=0.3$	–	$-0.09 \pm 0.02$

Table 4. The number of experimental events ( $N_{\text{event}}$ ) and  $\pi^-$ -mesons ( $N_{\pi^-}$ ), the asymmetry coefficient ( $\xi$ ), the strength of the correlation ( $\zeta$ ) and the mean rapidity ( $\langle y \rangle$ ) of  $\pi^-$ -mesons.

$A_P - A_T$	$N_{\text{event}}$	$N_{\pi^-}$	$\xi$	$\zeta$	$\langle y \rangle$
CNe	723	6209*	$-0.08 \pm 0.02$	$0.85 \pm 0.08$	$1.17 \pm 0.06$
MgMg	6239	50775	$-0.09 \pm 0.02$	$0.84 \pm 0.09$	$1.23 \pm 0.07$
CCu	1866	12390	$0.12 \pm 0.03$	$1.29 \pm 0.27$	$0.93 \pm 0.06$
OPb	732	7023	$0.23 \pm 0.05$	$1.61 \pm 0.35$	$0.73 \pm 0.07$

\* -  $\pi^+$  mesons are included also.



"INELASTIC" TRIGGER =  $S_1 \wedge S_2 \wedge S_3 \wedge S_4 \wedge \bar{S}_5 \wedge \bar{S}_6$

"CENTRAL" TRIGGER =  $S_1 \wedge S_2 \wedge S_3 \wedge S_4 \wedge \bar{S}_n \wedge \bar{S}_{ch}$

Figure 1: Experimental set-up. The trigger and trigger distances are not to scale

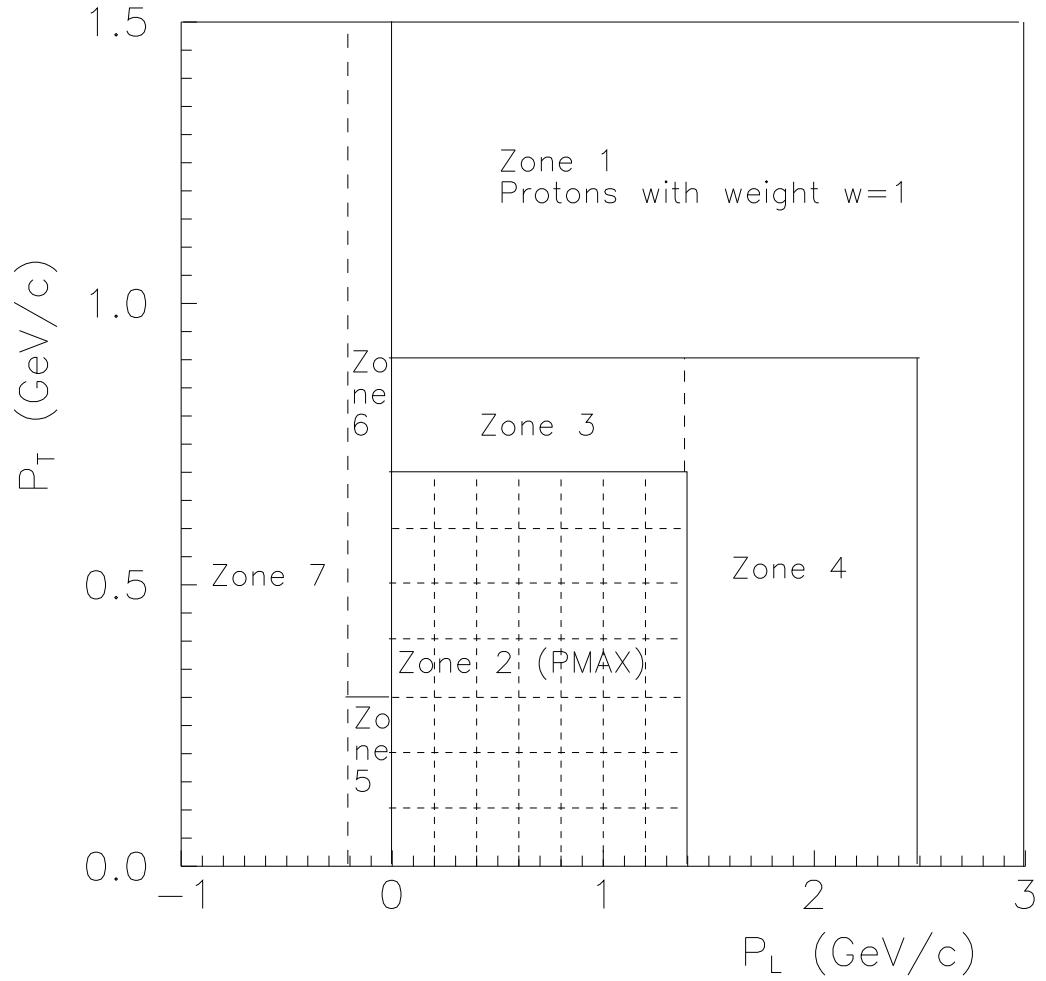


Figure 2: Two dimensional ( $p_T$ ,  $p_L$ ) ( $p_T$  and  $p_L$  denote the transverse and longitudinal momenta, correspondently) plot for the in CNe collisions for the identification of protons and  $\pi^+$  mesons.

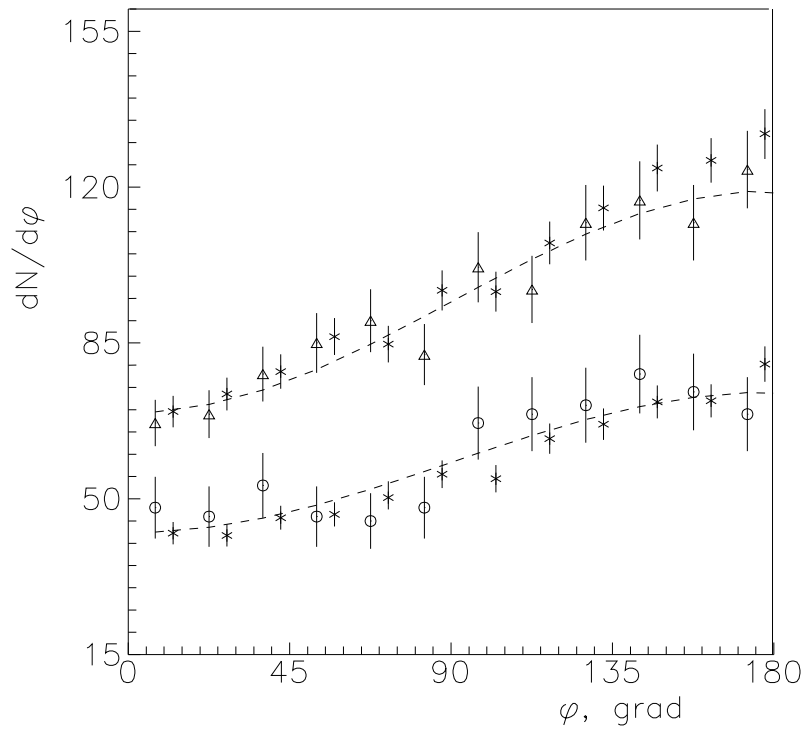


Figure 3: The dependence of the correlation function  $C(\Delta\varphi)$  on the  $\varphi$  for protons from: ( $\circ$ ) – CNe and ( $\Delta$ ) – CCu collisions. ( $\times$ ) – the QGSM data. Dashed curves are the results of the approximation of the data (see text).

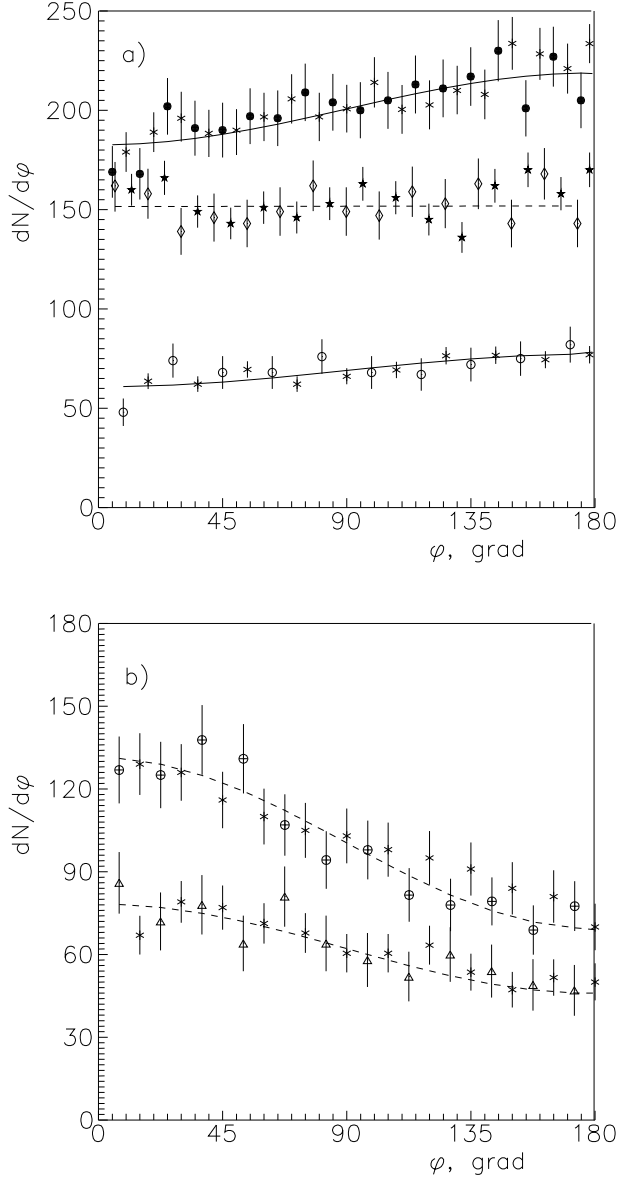


Figure 4: The dependence of the correlation function  $C(\Delta \varphi)$  on the  $\varphi$  for  $\pi^-$ -mesons from: (a) ( $\circ$ ) – CNe, ( $\bullet$ ) – MgMg ( $n_- \geq 7$ ), ( $\diamond$ ) – MgMg ( $n_- < 7$ ) and (b) ( $\triangle$ ) – CCu, ( $\oplus$ ) – OPb collisions. ( $\times$ ,  $\star$ ) – the QGSM data, correspondently. Solid and dashed curves are the results of the approximation of the data (see text).



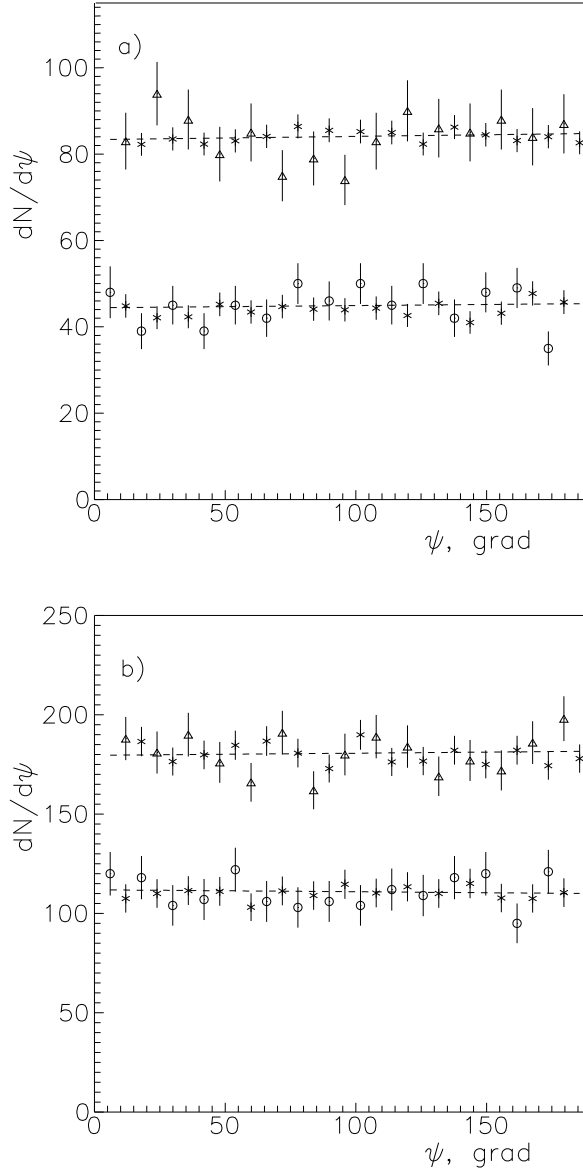


Figure 5: The dependence of the correlation function  $C(\Delta\psi)$  on the  $\psi$  in CCu collisions for protons (a) and for  $\pi^-$ -mesons (b). (o) – for particles emitted in the backward hemisphere, ( $\Delta$ ) – for particles emitted in forward hemisphere. ( $\times$ ) – the QGSM data. Curves are the results of the approximation of the data by the first order polynomials.

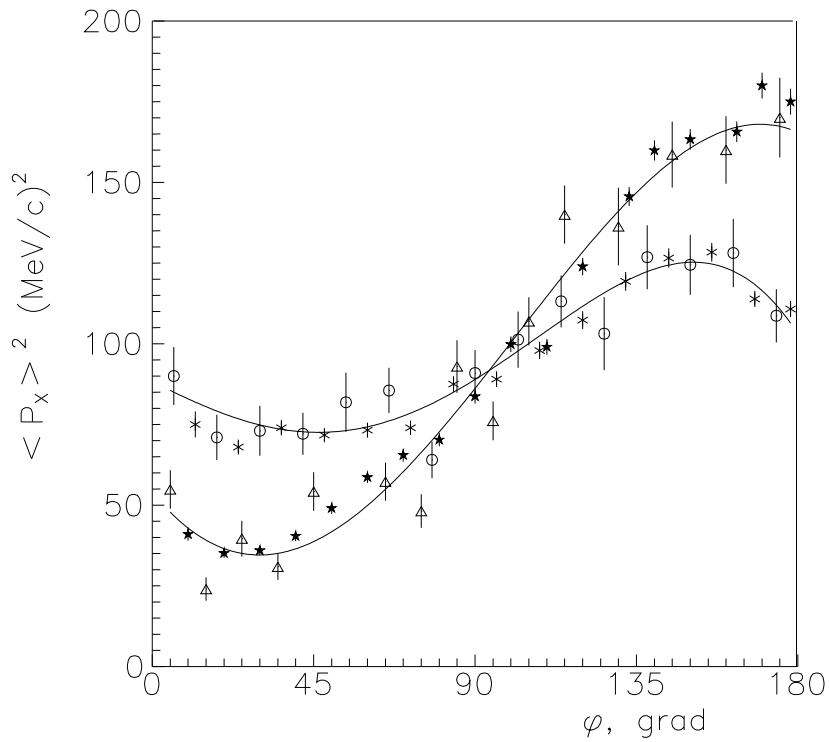


Figure 6: The dependence of  $\langle P_x \rangle^2$  on  $\varphi$  (as described in the text) for protons in: (o) – CNe and ( $\Delta$ ) – CCu collisions. ( $\times$ ,  $\star$ ) – the QGSM data, correspondently. Solid curves are the results of the approximation data by 4th order polynomials.